Precise stellar ages: combining isochrone fitting with empirical gyrochronology

Ruth Angus[1,2,], Timothy D. Morton[3,2,], Dan Foreman-Mackey[2], Jason Curtis[4], Stephen Kane[5], Megan Bedell[2], David W. Hogg[6,2,8] John Brewer[9], Rocio Kiman[10], & Jen van Saders[11]

ABSTRACT

[1]American Museum of Natural History, Central Park West, Manhattan, NY, USA

[2]Center for Computational Astrophysics, Flatiron Institute, 162 5th Avenue, Manhattan, NY, USA

[3]Department of Astronomy, University of Florida, Gainesville, FL, USA

[5]Department of Physics and Astronomy, UC Riverside, Riverside, CA, USA

[4]Department of Astronomy, Columbia University, Manhattan, NY, USA

[6]Center for Cosmology and Particle Physics, New York University, Manhattan, NY, USA

[7]Center Data Science, New York University, Manhattan, NY, USA

[8]Max-Planck Institute for Astronomy, Königstuhl, Heidelberg, Germany

[9]Yale center for astronomy and astrophysics, Yale University, New Haven, CT, USA

[10]Department of physics, CUNY Graduate Center, City University of New York, Manhattan, NY, USA

[11]Institute for Astronomy, University of Hawai'i at Mānoa, Honolulu, HI, USA

We present a new technique that combines two different established age-dating methods: gyrochronology and isochrone fitting to infer precise stellar ages. This method provides ages with 20% precision across the MS and subgiant branch. Gyrochronology and isochrone fitting are independent age-dating methods, each capable of providing extremely precise ages in certain areas of the Hertzsprung-Russell diagram. Combined, they can be applied to a much broader range of stellar masses and evolutionary stages and can provide ages that are more precise and accurate than either method in isolation. Rotation periods supply precise ages for cool stars on the main sequence via gyrochronology and isochrone fitting provides precise ages near main sequence turn off. In this investigation, we demonstrate that the observables of main sequence stars used to trace core hydrogen burning and stellar evolution on the Hertzprung-Russell diagram ($T_{\rm eff}$, [Fe/H], log(g), parallax, apparent magnitude and photometric colors) can be combined with *Kepler* rotation periods, in a Bayesian framework, to infer precise stellar ages from both isochrone fitting and gyrochronology simultaneously. We show that incorporating rotation periods into stellar evolution models significantly improves the precision of inferred ages on the main sequence. However, since ages predicted with gyrochronology on the main sequence are, in general, much more precise than isochronal ages, care must be taken to ensure the gyrochronology relation being used is accurate. The goal of this study is to explore the power of combining two independent dating methods, not to recalibrate or improve upon existing gyrochronology models. However, only a slight modification to our algorithm would be required to perform a calibration and, since the code is modular, an updated gyrochronology model could easily replace the one used here in future. This publication is accompanied by open source code (*Python* package, `stardate`), for inferring stellar ages for cool main sequence stars and subgiants from rotation periods, spectroscopic parameters and/or apparent magnitudes and parallaxes.

1. Introduction

The formation and evolution of the Milky Way and the planetary systems within it are two topics of significant interest in astronomy today. Both of these fields require precise and accurate ages for tens to hundreds of thousands of stars, however, age is the most

difficult stellar property to measure. The difficulty of age-dating is particularly acute for low mass (GKM) stars on the MS, precisely those that comprise the majority of known planet hosts. Using conventional dating methods, uncertainties on the ages of these stars can be as large as the age of the Universe. The stars eligible for *truly* precise age-dating, where age uncertainties can be as low as 10%, are those in nearby open clusters, those with observable acoustic oscillations (asteroseismic stars), those just turning off the MS, and the Sun (see Soderblom 2010, for a review of stellar ages). There are only a few tens of cool, MS stars with precise ages that are suitable for exoplanet population studies, however *tens-of-thousands* of precise ages are needed to study the evolution of planetary systems (*e.g.* Petigura et al. 2013; Foreman-Mackey et al. 2014; Veras et al. 2015; Burke et al. 2015). The number of planets detected in open clusters, and therefore with precise ages, is growing (*e.g.* Mann et al. 2017; Rizzuto et al. 2018; Vanderburg et al. 2018; Mann et al. 2018), however there are still only a couple of dozen of these discovered so far and the total number of detectable planets in clusters is unlikely to reach statistical numbers in the near future. In order to study the evolution of planetary systems, a significant number of precise ages for cool MS *field* stars are needed.

The ages of GKM dwarfs are difficult to measure because their spectra and colors of MS stars do not change rapidly. This is represented in the spacing of isochrones on a Hertzsprung-Russell (HR) or color-magnitude diagram (CMD). On the MS, isochrones are tightly spaced and, even with very precise measurements of effective temperature and luminosity, the position of a MS star on the HR diagram may be consistent with range of isochrones spanning several billion years. At main sequence turn-off however, isochrones are spread further apart, so that sufficiently precisely measured temperatures and luminosities can yield ages that are extremely precise. The classical method for measuring stellar ages is isochrone placement, or isochrone fitting, where surface gravity changes resulting from fusion in the core (usually observed via luminosity, L, and effective temperature, $T_{\rm eff}$, or absolute magnitude and colour) are compared with a set of models that trace stellar evolution across the HR diagram, or CMD. Surface gravity changes have been thoroughly mapped with physical models, and can be used to calculate relatively accurate, but not necessarily precise, ages, barring some small, $\sim$10% variations between different models (*e.g.* Yi et al. 2001; Dotter et al. 2008; Dotter 2016). Isochronal ages *can* be precise for stars turning off the MS, because the rate of change in brightness and temperature is large during this phase of stellar evolution. However, on the MS itself, there is little differentiation between stars of different ages in the L and $T_{\rm eff}$ plane, so ages tend to be very imprecise. The method of inferring a star's age from its rotation period, called 'gyrochronology', is much better suited for measuring ages on the MS because MS, stars spin down relatively rapidly.

Magnetic braking in MS stars was first observed by Skumanich (1972) who, studying

young clusters and the Sun, found that the rotation periods of Solar-type stars decay with the square-root of time. It has since been established that the rotation period of a star depends, to first order, only on its age and mass (*e.g.* Barnes 2003). This means that by measuring a star's rotation period and a suitable mass proxy (B-V color is commonly used), one can determine its age. The convenient characteristic of stars that allows their ages to be inferred from their *current* rotation periods and independently of their primordial ones, comes from the steep dependence of spin-down rate on rotation period (Kawaler 1989). This means that a star spinning with high angular velocity will experience a much greater angular momentum loss rate than a slowly spinning star. For this reason, no matter the initial rotation period of a Sun-like star, after around the age of the Hyades (500-700 million years) stellar rotation periods appear to converge onto a tight sequence (Irwin and Bouvier 2009). After this time, the age of a star can be inferred, to first order, from its mass and rotation period alone and this is the principle behind gyrochronology.

The relation between age, rotation period and mass has been studied in detail, and several different models have been developed to capture the rotational evolution of Sun-like stars. Some of these models are theoretical and based on physical processes; modeling angular momentum loss as a function of stellar properties as well as the properties of the magnetic field and stellar wind (Kawaler 1988, 1989; van Saders and Pinsonneault 2013; Matt et al. 2015; van Saders et al. 2016). Other models are empirical and capture the behavior of stars from a purely observational standpoint, using simple functional forms that can reproduce the data (Barnes 2003, 2007; Mamajek and Hillenbrand 2008; Angus et al. 2015). Both types of model, theoretical and empirical, must be calibrated using observations. Old calibrators are especially important because new evidence suggests that rotational evolution goes through a transition at old age or, more specifically, at a large Rossby number, Ro (the ratio of rotation period to the convective overturn timescale). For example, old *Kepler* asteroseismic stars rotate more rapidly than expected given their age (*e.g.* Angus et al. 2015; van Saders et al. 2016). A new physically motivated gyrochronology model, capable of reproducing these data, was recently introduced (van Saders et al. 2016). It relaxes magnetic breaking at a critical Rossby number of around 2, approximately the Solar value. This model predicts that, after stellar rotation periods lengthen enough to move stars cross this Ro threshold, stars stop spinning down and maintain a constant rotation period from then until they evolve off the MS. The implication is that the ages of stars with $Ro > 2.1$ cannot be measured from their rotation periods.

The gyrochronology models that capture post Ro-threshold, rotational evolution (van Saders et al. 2016) are the current state-of-the-art in rotation dating. These models are expensive to compute and, just as with most isochrones and stellar evolution tracks, are usually pre-computed over a grid of stellar parameters, then interpolation is used to pre-

dict the age of a star. The process of measuring a stellar age with these models is similar to inferring an age using any set of isochrones, with the main difference being that rotation period is an additional dimension. Ages calculated using these models are therefore likely to be much more precise than using rotation-free isochrones since rotation period provides an additional anchor-point for the age of a star. We present here a complementary method that combines isochrones with an *empirical* gyrochronology model using a Bayesian framework. The methodology is related to the models described above (van Saders et al. 2016) in that both use a combination of rotation periods and other observable properties that track stellar evolution on the HR diagram in concert. The main difference is that the gyrochronology model used here is an entirely empirically calibrated one, as opposed to a physically derived one. One major advantage of using a physically motivated gyrochronology model over an empirically calibrated one is the ability to rely on physics to interpolate or extrapolate over parts of parameter space with sparse data coverage. However, rotational spin-down is a complex process that is not yet fully understood and currently no physical model can accurately reproduce all the data available. For this reason, even physically motivated gyrochronology models cannot always be used to reliably extrapolate into unexplored parameter space. Physical models, when calibrated to data. can provide insight into the physics of stars however, if accurate and precise *prediction* of stellar properties is desired, empirical models can have advantages over physical ones. For example, the data may reveal complex trends that cannot be reproduced with our current understanding of the physical processes involved but may be captured by more flexible data-driven models. In addition, it is relatively straightforward to build an element of stochasticity into empirical models, *i.e.* to allow for and incorporate outliers or noisy trends. This may be particularly important for stellar spin down, which does not always seem to behave predictably. A further advantage of empirical models is that inference is more tractable: it can be extremely fast to fit them to data. We use a simple, empirical, deterministic gyrochronology model in this work, which, like any other gyrochronology model, cannot yet reproduce all the observed data. Simple modifications could be made to this model to produce significant improvements, for example, by including a mixture model to account for outliers and binaries, however we leave these improvements for a future project. Ultimately, the model we present here will provide a baseline against which other gyrochronology models can be compared. We also provide a new gyrochoronology *Python* package, the first of its kind, called `stardate` which accompanies this paper.

There are several reasons why combining isochrone fitting with gyrochronology is more powerful than using either method in isolation. Firstly, the two methods are optimal in different parts of the HR diagram: gyrochronology works well for FGK dwarfs and isochrone fitting works well for subgiants and hot stars, so combining the two methods results in

consistently precise ages across a range of masses, ages and evolutionary stages. Secondly, using both methods at once circumvents the need to decide which method to use *a priori*. It eliminates the circular process of classifying a star based on its CMD position (M dwarf, subgiant, etc), then deciding which age-dating method to use, then inferring an age which itself depends on the classification that was made. It is important to infer all stellar properties at once since they all depend on each other. Thirdly, including a rotation period measurement can actually improve mass and metallicity estimates since these properties depend on stellar age.

This paper is laid out as follows. In section 2 we describe our new age-dating model and its implementation, in section 3 we test this model on simulated stars and cluster stars, and in section 4 we discuss the implications of these tests and future pathways for development. Throughout this paper we use the term *'observables'* to refer to the following observed properties of a star, $T_{\rm eff}$, log(g), observed bulk metallicity ($[\hat{F}]$), parallax ($\bar{\omega}$), photometric colors in different passbands ($\mathbf{m_x} = [m_J, m_H, m_K, m_B, m_V, m_G, ...]$, etc) and rotation period ($P_{\rm rot}$). The term *'parameters'* refers to the physical properties of that star: age (A), equivalent evolutionary point (EEP), true bulk metallicity (F), distance (D) and V-band extinction (A_V). These are the properties that generate the observables.

2. Method

In this section we describe our combined isochrone fitting and gyrochronology model. Combining information from different models can be relatively simple, as long as the processes being modeled; those that generated the data, are independent. In this case, we are combining information that relates to the burning of hydrogen in the core, which translates to CMD position, with information about the magnetic braking history of a star (the current rotation period). We can assume that, to first order, these two processes are independent: the hydrogen fraction in the core does not affect a star's rotation period and vice versa. In practise, we can never be entirely sure that two such processes are independent but, at least within the uncertainties, any dependence here is unlikely to affect our results. If this assumption is valid, the likelihoods calculated using each model can be multiplied together.

The desired end product of this method is an estimate of the non-normalized posterior probability density function (PDF) over the age of a star,

$$p(A|\mathbf{m_x}, T_{\rm eff}, \log(g), \hat{F}, P_{\rm rot}, \bar{\omega}), \tag{1}$$

where A is age, $\mathbf{m_x}$ is a vector of apparent magnitudes in various bandpasses, $\hat{F}$ is the *observed* bulk metallicity, $P_{\rm rot}$ is the rotation period and $\bar{\omega}$ is parallax. In order to calculate a posterior PDF over age, we must marginalize over parameters that relate to age, but are not of interest in this study. These parameters include equivalent evolutionary point (EEP), which is a dimensionless number ranging from around 200 for M dwarfs up to around 500 for subgiants and is 355 for the Sun (see Dotter 2016; Choi et al. 2016). Stars are defined as subgiants when their EEP exceeds 454. Mass can be calculated from EEP, age and metallicity. The other parameters are distance (D), V-band extinction (A_V) and the *inferred* bulk metallicity, F. The marginalization involves integrating over these extra parameters,

$$\begin{aligned} &p(A|\mathbf{m_x}, T_{\rm eff}, \log(g), \hat{F}, P_{\rm rot}, \bar{\omega}) \\ &\propto \int p(\mathbf{m_x}, T_{\rm eff}, \log(g), \hat{F}, P_{\rm rot}, \bar{\omega}|A, EEP, D, A_V, F)\ p(A)p(EEP)p(D)p(A_V)p(F)dEEPdDdA_VdF. \end{aligned} \tag{2}$$

This equation is a form of Bayes' rule,

$$\text{Posterior} \propto \text{Likelihood} \times \text{Prior}, \tag{3}$$

where the likelihood of the data given the model is,

$$p(\mathbf{m_x}, T_{\rm eff}, \log(g), \hat{F}, \bar{\omega}, P_{\rm rot}|A, EEP, D, A_V, F), \tag{4}$$

and the prior PDF over parameters is,

$$p(A)p(EEP)p(D)p(A_V)p(F). \tag{5}$$

Not all of the observables on the left of the '|' in the likelihood depend on all of the parameters to the right of it. For example, rotation period, $P_{\rm rot}$ does not depend on V-band extinction, A_V. In our model, we make use of conditional independencies like this and use them to factorize the likelihood. Instead of the likelihood of equation 9, where every observable depends on every parameter, our model can be factorized as,

$$p(\mathbf{m_x}, T_{\rm eff}, \log(g), \hat{F}, \bar{\omega}|A, EEP, D, A_V, F, C_{B-V}, M)\ p(P_{\rm rot}|A, C_{B-V}, M), \tag{6}$$

where we have introduced two new parameters, C_{B-V}, which is the $B-V$ color that is often used as a mass proxy in the literature and mass itself (M), which is used in our gyrochronology model. The above factorization of the likelihood describes the fact that, in our model, rotation period does not depend directly on $T_{\rm eff}$, distance, etc, but on C_{B-V}, mass and age. It is the EEP, age, metallicity, extinction and distance that determines the observed spectroscopic properties ($T_{\rm eff}$, log(g), [Fe/H]) and apparant magnitudes, $\mathbf{m_x}$). These parameters also determine the C_{B-V} color and mass of a star. In turn, it is a star's age C_{B-V} color and mass that determine its rotation period. Written this way, stellar rotation periods do not directly depend on stellar mass. This likelihood function does not necessarily represent the physical realities of stellar evolution, however breaking up the problem this way allows us to easily combine isochronology and gyrochronology and infer the joint age of a star from all its observables. While true that rotation period also depends on EEP and metallicity at some level, we assume that these dependencies are weak enough not to significantly affect the ages that we infer.

The factorization of the likelihood described in equation 6 allows us to multiply two separate likelihood functions together: one computed using an isochronal model and one computed using a gyrochronal model. We assume that the probability of observing the measured observables, given the model parameters is a Gaussian and that the observables are identically and independently distributed, so we use Gaussian likelihood functions. The isochronal likelihood function is,

$$\begin{aligned}\mathcal{L}_{\rm iso} &= p(\mathbf{m_x}, T_{\rm eff}, \log(g), \hat{F}, \bar{\omega}, C_{B-V}|A, \mathrm{EEP}, D, A_V, F) \\ &= \frac{1}{\sqrt{(2\pi)^n \det(\Sigma)}} \exp\left(-\tfrac{1}{2}(\mathbf{O_I}-\mathbf{I})^T\Sigma^{-1}(\mathbf{O_I}-\mathbf{I})\right),\end{aligned} \tag{7}$$

where $\mathbf{O_I}$ is the n-dimensional vector of n observables: $T_{\rm eff}$, log(g), $\hat{F}$, $\bar{\omega}$, $\mathbf{m_x}$ (where n is 4 plus the number of apparant magnitudes in different pass-bands that are available) and Σ is the covariance matrix of that set of observables. $\mathbf{I}$ is the vector of *model* observables that correspond to a set of parameters: A, EEP, F, D and A_V, calculated using an isochrone model. We assume there is no covariance between these observables and so this covariance matrix consists of individual parameter variances, added in quadrature to an additional

variance that depends on B-V color and evolutionary stage, along the diagonal with zeros everywhere else. The additional variance is described in more detail later in this section. The gyrochronal likelihood function is,

$$\begin{aligned} \mathcal{L}_{\rm gyro} &= p(P_{\rm rot}|A, C_{B-V}, M) \\ &= \frac{1}{\sqrt{(2\pi)\det(\Sigma_P)}} \exp\left(-\frac{1}{2}(\mathbf{P_O} - \mathbf{P_P})^T \Sigma^{-1} (\mathbf{P_O} - \mathbf{P_P})\right), \end{aligned} \tag{8}$$

where $\mathbf{P_O}$ is a 1-D vector of observed log-rotation periods, $\mathbf{P_P}$ is the vector of corresponding predicted log-rotation periods, calculated using the vector of ages and C_{B-V} values that correspond to the input parameters as predicted by the isochronal model. The full likelihood function used in our model is the product of these two likelihood functions,

$$\begin{aligned} \mathcal{L}_{\rm full} &= \frac{1}{\sqrt{(2\pi)^n \det(\Sigma)}} \exp\left(-\frac{1}{2}[\mathbf{O_I} - \mathbf{I}]^T \Sigma^{-1} [\mathbf{O_I} - \mathbf{I}]\right) \\ &\times \frac{1}{\sqrt{(2\pi)\det(\Sigma_P)}} \exp\left(-\frac{1}{2}[\mathbf{P_O} - \mathbf{P_P}]^T \Sigma^{-1} [\mathbf{P_O} - \mathbf{P_P}]\right). \end{aligned} \tag{9}$$

We placed priors over the model parameters A, EEP, F, D and A_V. These distributions, described in the appendix, represent our prior beliefs about the values these parameters will take, before using the data to update those beliefs via a likelihood and produce a posterior belief about their values.

To calculate $\mathbf{I}$, the vector of predicted isochronal observables, we used the `isochrones.py` *python* package which has a range of functionalities relating to isochrone fitting. The first of the `isochrones.py` functions we used is the likelihood function of equation 7. The `isochrones.py` likelihood function accepts a dictionary of observables which can, but does not *have* to include, all of the following: $T_{\rm eff}$, log(g), F, parallax and apparent magnitudes in a range of colors, as well as the uncertainties on all these observables. It then calculates the residual vector $(\mathbf{O_I} - \mathbf{I})$ where $\mathbf{O_I}$ is the vector of observables and $\mathbf{I}$ is a vector of corresponding predicted observables. The prediction is calculated using a set of isochrones (we used the MIST models, Paxton et al. 2011, 2013, 2015; Dotter 2016; Choi et al. 2016; Paxton et al. 2018), where the set of *model* observables that correspond to a set of physical parameters is returned. This requires interpolation over the model grids since, especially at high dimensions, it is unlikely that any set of physical parameters will exactly match a precomputed set of isochrones. The observables that correspond to a set of physical parameters go into $\mathbf{I}$ and the `isochrones.py` likelihood function returns the result of equation 7. The second `isochrones.py` function we used is one that predicts C_{B-V} for a given set of stellar parameters, which was then used to calculate the gyrochronal likelihood function of equation 8.

The inference processes procedes as follows (as a reminder, we use *observables* to refer to the data: $T_{\rm eff}$, log(g), etc and *parameters* to refer to the model parameters: EEP, age, metal-

licity, distance and extinction. First, a set of parameters: age, EEP, metallicity, distance and extinction, as well as observables $T_{\rm eff}$, log(g), bulk metallicity, apparent magnitudes and parallax ($\mathbf{O_I}$) for a single star are passed to the isochronal likelihood function, equation (7). Then, a set of *model* values of $T_{\rm eff}$, log(g), bulk metallicity, apparent magnitudes and parallax ($\mathbf{I}$) that correspond to that set of parameters are calculated by `isochrones.py`. The isochronal log-likelihood, $\ln(\mathcal{L}_{\rm iso})$, is then computed for these parameter values. The same age that was passed to the likelihood function, and the C_{B-V} and mass corresponding to it, along with the observed rotation period, are then passed to the gyrochronal likelihood function (equation 8). The gyrochronal log-likelihood, $\ln(\mathcal{L}_{\rm gyro})$, is computed. The full log-likelihood is then calculated,

$$\ln(\mathcal{L}_{\rm full}) = \ln(\mathcal{L}_{\rm iso}) + \ln(\mathcal{L}_{\rm gyro}), \tag{10}$$

and added to the log-prior to produce a single sample from the posterior PDF.

The gyrochronology model used to predict $\mathbf{P_P}$ was,

$$P_{\rm rot} = \begin{cases} A^{\eta}\alpha(C_{B-V} - \delta)^{\beta}, & \text{if } Ro < 2. \\ P_{\rm max}, & \text{if } Ro \geq 2. \end{cases} \tag{11}$$

where $P_{\rm rot}$ is rotation period in days, C_{B-V} is a star's $B-V$ color, A is stellar age in Myrs and η, α, β and δ take values 0.55, 0.4, 0.31 and 0.45 respectively (Angus et al. 2015). This functional form was introduced by (Barnes 2007) and the parameter values are adopted from the recalibration performed in Angus et al. (2015), which is based on young cluster stars and old asteroseismic stars. We adapted this classical gyrochronology model to incorporate the new observations showing that magnetic braking ceases at a critical Rossby number (van Saders et al. 2016). The Rossby number, Ro, is the ratio of rotation period to convective overturn time $P_{\rm rot}/\tau$ and determines whether a star is still undergoing magnetic braking ($Ro < 2$) or has stopped spinning down and retains its terminal rotation period, $P_{\rm max}$, which is the period it had as it reached the critical Rossby number of 2 (van Saders et al. 2016). The convective overturn time, τ, was estimated using equation 11 of Wright et al. (2011). Figure 1 shows the rotation periods of 841 simulated stars with rotation periods generated from the gyrochronology model.

The rotation periods of hot stars, cool stars, subgiants and giants evolve differently to FGK and early M dwarfs. Stars more massive than around 1.25 $M_\odot$, with a temperature $\gtrsim$ 6250 K and a $B-V$ color $\lesssim$ 0.45 do not spin down appreciably over their main sequence lifetimes since they do not have the deep convective envelope needed to generate strong magnetic fields. Late M dwarfs with masses $\lesssim$ 0.3 $M_\odot$, temperatures $\lesssim$ 3500 and $B-V$ $\gtrsim$ 1.4 do not start magnetic braking until at least after the age of Praesepe (∼650 million

Fig. 1.— The rotation period model. Late F, GK and early M dwarfs follow the Angus et al. (2015) gyrochronology relation, with the exception of old, slowly rotating stars with large Rossby numbers whose rotation periods are fixed at 2× their convective overturn time. The rotation periods of early F, late M dwarfs and subgiants were generate from a log-normal distribution with standard deviation shown in figure 2. The top panel shows the rotation periods vs. B-V colors of simulated stars, colored by their age and the bottom panel shows the same stars colored by their equivalent evolutionary point (EEP). The gray lines describe the (Angus et al. 2015) gyrochronology model.

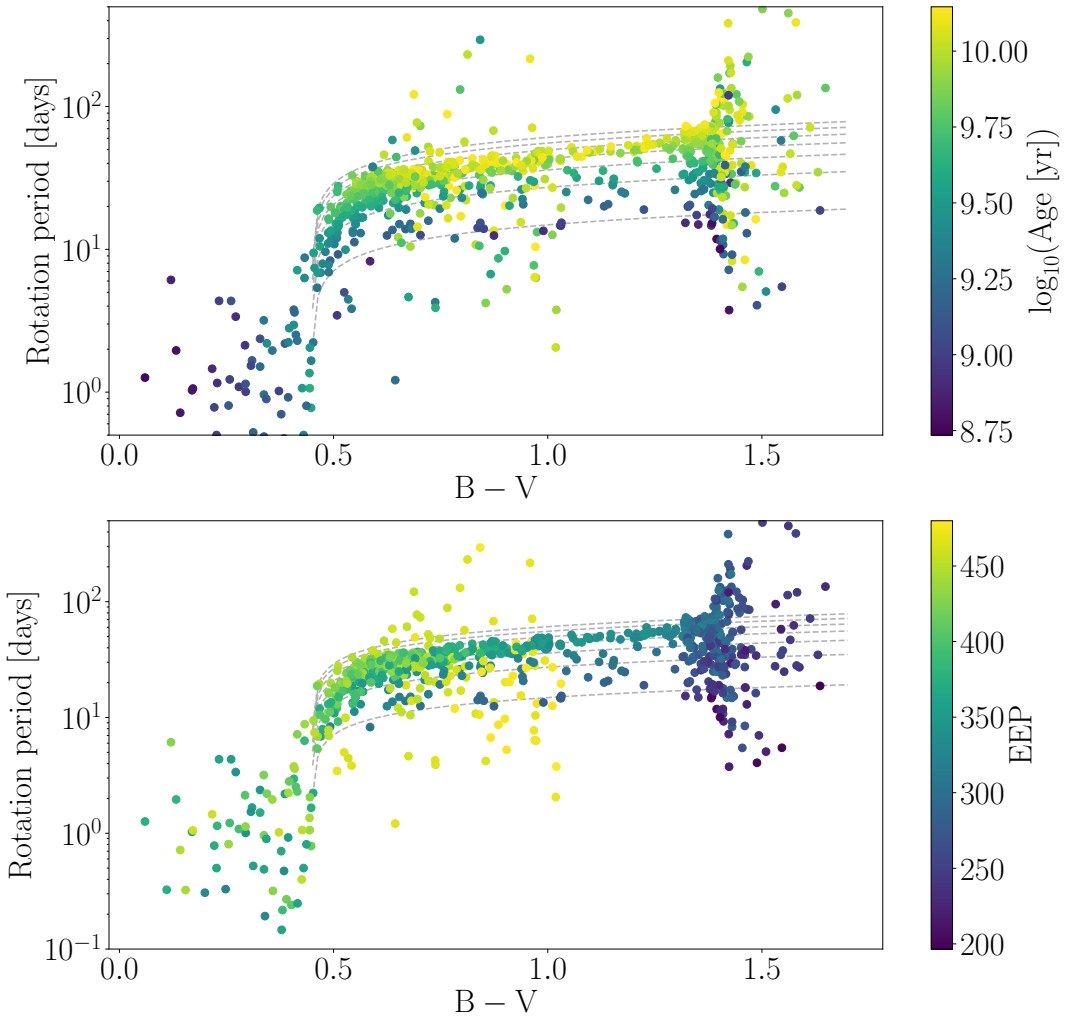

years). Both hot and cool stars retain rotation periods that are similar to their primordial distribution (see *e.g.* Matt et al. 2012). Finally, the rotation periods of evolved stars slow dramatically as their radii grow. The empirical gyrochronology relation described above does not include these stars, however it is still possible to infer the ages of hot and evolved stars using isochrone fitting (unfortunately neither gyrochronology nor isochrone fitting works well for late M dwarfs). In order to 'switch off' gyrochronology, and just use isochrone fitting for the hot, cool and evolved stars, we designed a model describing the rotation period variance of these stars, inflating the variance to high values in regions of parameter space where gyrochronology does not apply. The variance model was designed to reflect the observed distributions of hot, cool and evolved stars, however its main purpose is to artificially reduce the amount of age-information carried by rotation periods for stars where the rotation period is uninformative. We used three sigmoid functions to increase the standard deviation of the rotation period distributions of hot, cool and evolved stars which are shown in figure 2. This additional variance is zero where gyrochronology works well: FGK and early M dwarfs and 0.25 ($\sigma = 0.5$) for hot, cool and evolved stars. The logistic functions shown in figure 2 reach half their maximum values at 0.45, 1.4 and 454 for hot stars, cool stars and subgiants, respectively. The maximum standard deviation value of all three groups (hot, cool and evolved) is 0.5 and the logistic growth rate, or steepness, of the three sigmoids are 100, 100 and .2 for hot, cool and evolved stars respectively. If a star is both hot and evolved, the additional standard deviation of its rotation period will rise to 1 (no late M dwarfs have yet evolved off the main sequence so this will not apply to the cool stars). The (log) rotation periods of hot stars are modelled as a broad Gaussian with a mean of 0 (1 day in linear rotation period) and a standard deviation of 0.5. The (log) rotation periods of cool and evolved stars were modelled as a Gaussian with mean given by the log of equation 11 and standard deviations of 0.5.

When applying our model to infer the age of a star, we sampled the joint posterior PDF over age, mass, metallicity, distance and extinction using the affine invariant ensemble sampler, `emcee` (Foreman-Mackey et al. 2013) with 24 walkers. Samples were drawn from the posterior PDF until 100 *independent* samples were obtained. We actively estimated the autocorrelation length, which indicates how many steps were taken per independent sample, after every 100 steps using the autocorrelation tool built into `emcee`. The MCMC concluded when *either* 100 times the autocorrelation length was reached and the change in autocorrelation length over 100 samples was less than 0.01, *or* the maximum of 100,000 samples was obtained. This method is trivially parallelizable, since the inference process for each star can be performed on a separate core. The age of a single star can be inferred in around 10 minutes on a laptop computer.

Fig. 2.— The additional standard deviation in rotation period added to the observational period uncertainties in our model. The standard deviation was artificially increased for early F stars ($B-V < 0.45$), late M dwarfs ($B-V > 1.4$) and evolved stars (EEP > 454) in order to down-weight the age-information supplied by rotation periods. The rotation periods of these stars do not follow the deterministic gyrochronology relation and their ages should mostly be inferred via isochrone fitting. Down-weighting the gyrochronal likelihood by the inverse variance ($1/\sigma^2$) allows the ages of these stars to be mostly inferred via isochrone fitting. The ages of hot and evolved stars can be relatively precisely constrained with isochrone fitting since their position on the CMD changes rapidly with time, however isochrone fitting cannot constrain the ages of late M dwarfs, so the age of any star with $B - V > 1.4$ will not be precisely constrained with `stardate`.

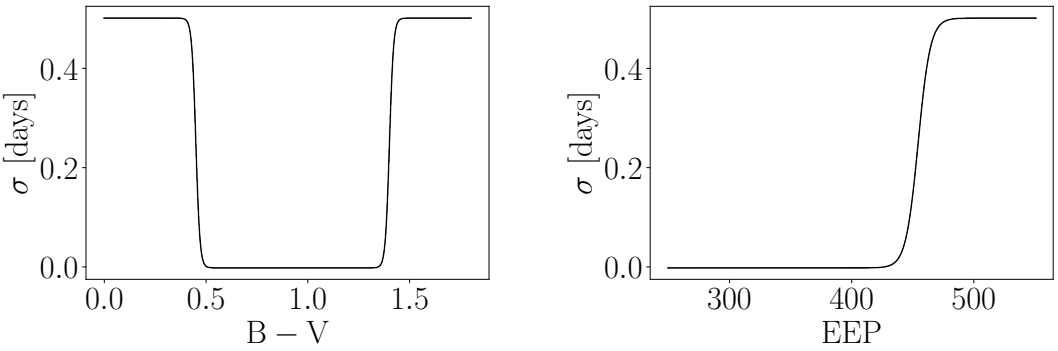

3. Results

In order to demonstrate the performance of our method, we conducted two sets of tests. In the first we simulated a set of observables from a set fundamental parameters for a few hundred stars using the MIST stellar evolution models and a gyrochronology model, then compared the parameters predicted with our model to the true parameters used to generate the data. In the second we tested our model by measuring the ages of individual stars in the Praesepe open cluster. The age of Praesepe has been measured precisely because it is an ensemble of coeval stars with the same metallicity: a single stellar poplulation, and its age can be precisely established through isochrone fitting and MS turn-off. We adopted an age of 650 Myrs for Praesepe (Fossati et al. 2008).

3.1. Test 1: simulated stars

For the first test we drew masses, ages, bulk metallicities, distances and extinctions at random for 1000 stars from the following uniform distributions:

$$\mathrm{EEP} \sim U(198, 480) \tag{12}$$

$$A \sim U(0.5, 14)\ [\mathrm{Gyr}] \tag{13}$$

$$F \sim U(-0.2, 0.2) \tag{14}$$

$$D \sim U(10, 1000)\ [\mathrm{pc}] \tag{15}$$

$$A_V \sim U(0, 0.1). \tag{16}$$

$T_{\rm eff}$, log(g), $\hat{F}$, parallax, and apparent magnitudes B, V, J, H, K, *Gaia* G, G_{BP} and G_{RP} were generated from these stellar parameters using the MIST stellar evolution models. We added a small amount of noise to the 'observed' stellar properties in order to reflect typical observational uncertainties. We added Gaussian noise with a standard deviation of 25 K to $T_{\rm eff}$, 0.01 dex to [Fe/H] and log(g), and 10 mmags to B, V, J, H, and K magnitudes. The noise added to Gaia G-band photometry ranged from 0.3 mmag for stars brighter than 13th magnitude, to 10 mmag for stars around 20th magnitude (Evans et al. 2017; Gaia Collaboration et al. 2018). Noise added to *Gaia* G_{BP} and G_{RP} bands ranged from 2 mmag for stars brighter than 13th magnitude to 200 mmag for stars fainter than 17th. Unphysical combinations of stellar parameters were discarded, resulting in a final sample size of 841 simulated stars. Figure 3 shows the position of these stars on an HR diagram (with log(g) on the y-axis instead of luminosity to improve the visibility of the MS), colored by their age. Rotation periods for FGK and early M dwarfs were generated using the gyrochronology relation of equation 11. Rotation periods for hot stars, cool stars

and subgiants were generated from Gaussian distributions (in log), with standard deviation described by the three sigmoid functions shown in figure 2. Based on the typical uncertainties on rotation periods in the McQuillan et al. (2014) catalog, we added Gaussian noise with a standard deviation of 1% to all stellar rotation periods.

We took two approaches to inferring the ages of these simulated stars: firstly using isochrone fitting *only*, and secondly using isochrone fitting *combined with* a gyrochronology model. Since the posterior PDFs of stars are often not unimodal, we found that the choice of initial positions of the `emcee` walkers influenced the final outcome because walkers occasionally got 'stuck' in certain areas of parameter space. We found that the following set of initial parameters worked well, though not perfectly, for FGK dwarfs but sacrificed some accuracy in subgiant ages: EEP = 330, $A = 9.56$ Gyr, $F = -0.05$, $D = 269$ pc and $A_V = 0.0$. Figure 4 shows the results of combining gyrochronology with isochrone fitting with simulated stars. The stars' true ages are plotted against their predicted ages, with `stardate` ages in color, and ages predicted using isochrone fitting only plotted in light grey. The five panels show the results for five different types of stars: late F, GK and early M dwarfs which are still undergoing magnetic braking (Ro < 2), late F, GK and early M dwarfs that have ceased magnetic braking (Ro > 2), hot stars ($B - V < 0.45$), cool stars ($B - V > 1.4$) and evolved stars (EEP > 454). As expected, the low *Ro*, FGK stars show the most drastic improvement in age precision. The median empirical age precision, the standard deviation of age posteriors as a percentage of age, was around 3% for this group and the median relative error, defined as the absolute difference between the true and age the inferred age, as a percentage of the true age, was less than 1%. The median error: the absolute difference between true and measured age was 30 Myrs. In contrast, the median empirical precision of ages measured using only isochrone fitting was 49% and the median error was 1.3 Gyr or 30%. Ages measured for FGK stars by combining gyrochronology and isochrone fitting with `stardate` were 50 times more accurate than ages measured with isochrone fitting. Even though the group of old FGK stars with large Rossby numbers have stopped magnetic braking, their rotation periods are still age-informative and relatively precise ages were measured for these stars with `stardate`. The median age precision for this group was 8% and 22% and the median age error was 300 Myr/3% and 1.3 Gyr/16% for ages measured with `stardate` and isochrone fitting respectively. Ages measured with `stardate` were over 4 times more accurate than ages measured with isochrone fitting only, so although these stars have stopped spinning down, their rotation periods are still highly age informative when paired with stellar evolution models. The median accuracy of hot star ages was marginally decreased with `stardate`, relative to isochrone fitting only (from a median error of 510 Myr to 560 Myr) because of issues with sampling the posterior PDFs. Adding gyrochronology to the age model creates a more multimodal posterior PDF which makes sampling more difficult, leading to some highly

inaccurate age measurements at very high and very low ages. The precision and accuracy of cool star and subgiant ages was relatively consistent for ages measured with stardate and ages measured with isochrone fitting only. This is expected because the rotation periods of these stars do not contain information about stellar ages. For the whole sample, combining gyrochronology and isochrone fitting results an overall age precision of 10% (down from 28% for isochrone fitting only), a median error of 340 Myrs (down from 1.3 Gyrs), and a relative error of 4% (down from 23 %). The ages of *all* FGKM dwarfs and subgiants are 3× more precise and 6× more accurate, on average, when their rotation periods are used to infer their ages.

Figure 5 shows the simulated stars on an HR diagram, with points colored by the relative precision of their predicted ages. log(g) is plotted the y-axis instead of luminosity because the MS spreads out more in $T_{\rm eff}$-log(g) space and it is easier to differentiate young and old stars. The top panel shows the precision of ages calculated using both gyrochronology and isochrone fitting and the bottom panel shows the precision of ages calculated with isochrone fitting only. Although these uncertainties are noisy (they are computed from the standard deviation of the age posteriors) they show that ages are extremely precise for young FGK stars, less precise for old FGK stars and relatively imprecise for late M dwarfs.

This simulation experiment is unrealistic for two main reasons: firstly, we simulated data from the same gyrochronology model we used to infer ages and so the results for FGK dwarfs are extremely accurate by design. Secondly, we simulated data without any noise or any additional instrinsic scatter for FGK dwarfs, resulting in ages with better precision than can be expected for real stars. Inaccuracies would arise if the gyrochronology model was incorrect or poorly calibrated in some areas of parameter space and imprecision would arise if excess intrinsic scatter were built into the gyrochronology model and/or the observations. We leave the recalibration of gyrochronology models for a future exercise since, in this work, we are mostly interested in testing the results of combining existing gyrochronology relations with isochrone fitting. The above experiment demonstrates that building gyrochronology into stellar evolution models results in much more precise age predictions, as predicted by information theory.

3.2. Test 2: the Praesepe Cluster

In order to test our model on real stars with known ages, we selected a sample of stars in the Praesepe open cluster. The ages of open clusters can be measured much more precisely than field stars because they formed from the same molecular cloud at the same time and therefore have the same metallicity and age (to within a few million years). Stars with

the same metallicity and age fall on the same isochrone, and provide a $N^{-1/2}$ decrease in age uncertainty where N is the number of cluster stars. Single stellar populations also allow main sequence turn off to be identified which provides a large amount of age information. We compiled rotation periods, *Gaia* photometry and *Gaia* parallaxes for members of Praesepe, a 650 Myr cluster (Fossati et al. 2008). We chose Praesepe because it is relatively tightly clustered on the sky and many of its members were targeted in a single *K2* campaign, from which rotation periods were measured via light curve frequency analysis (Douglas et al. 2017; Rebull et al. 2017). We identified Praesepe members with measured rotation periods from the Douglas et al. (2017) catalog in the *K2-Gaia* crossmatch catalog provided at `https://gaia-kepler.fun/`. This catalog cross-matched the EPIC catalog (Huber et al. 2016) with with the Gaia DR2 catalog (Gaia Collaboration et al. 2018), using a 1" search radius. The result was a sample of 757 stars with rotation periods, parallaxes and *Gaia* G, G_{BP} and G_{RP}-band photometry[12]. Figure 6 shows the rotation periods of Praesepe members as a function of their *Gaia* $G_{BP} - G_{RP}$ colors. FGK and early M stars, that lie tightly on the Praesepe isochrone and do not show excess luminosity suggestive of being a binary are shown as solid blue points. We only applied `stardate` to these stars because the purpose of this test was to demonstrate that it can predict accurate ages for stars that fall on the gyrochronology relation. `stardate` is not designed to predict precise ages for binary stars or other outliers. Figure 6 shows the posterior PDFs over age for the FGK and early M dwarf members of the praesepe cluster, calculated using `stardate`, compared with ages calculated using isochrone fitting (where each star was treated as a field star). The orange curves show the `stardate` posteriors and the blue curves show the isochrone-only posteriors. The blue PDFs are more tightly clustered around the established age of Praesepe ($\sim$ 650Myrs) than the orange PDFs because rotation periods were included in the age inference process.

The resulting probability density functions over age predicted for individual members of Praesepe, where each member was treated as an isolated field star, are shown in figure **??**. The orange distributions show posterior PDFs over age for each member of Praesepe, where ages were inferred using isochrone fitting *only*, with *Gaia* colors ($G_{BP} - G_{RP}$), *Gaia* apparent magnitude (G), and *Gaia* parallaxes as the observable properties. The blue distributions are posterior PDFs over stellar age for each member of Praesepe, where ages were inferred using isochrone fitting *and* a gyrochronology model (equation 11). The blue posteriors are much more strongly peaked around the literature age of the cluster (650 Myrs, indicated by a vertical black line) and this demonstrates that rotation periods carry substantially more age information than CMD position, even when precise parallaxes are available.

[12]This analysis was performed in a Jupyter notebook available here: `https://github.com/RuthAngus/stardate/blob/master/paper/code/Praesepe.ipynb`

In summary, fitting our new age model to simulated stars and members of the Praesepe cluster (an open cluster with a precisely measured age from ensemble isochrone fitting and MS turn-off) demonstrates that using isochrone fitting *alone* to calculate the ages of cool MS field stars results in extremely imprecise ages, however when gyrochonology is incorporated, the precision of age measurements increase significantly.

Fig. 3.— The simulated star sample plotted on an HR diagram and colored by age.

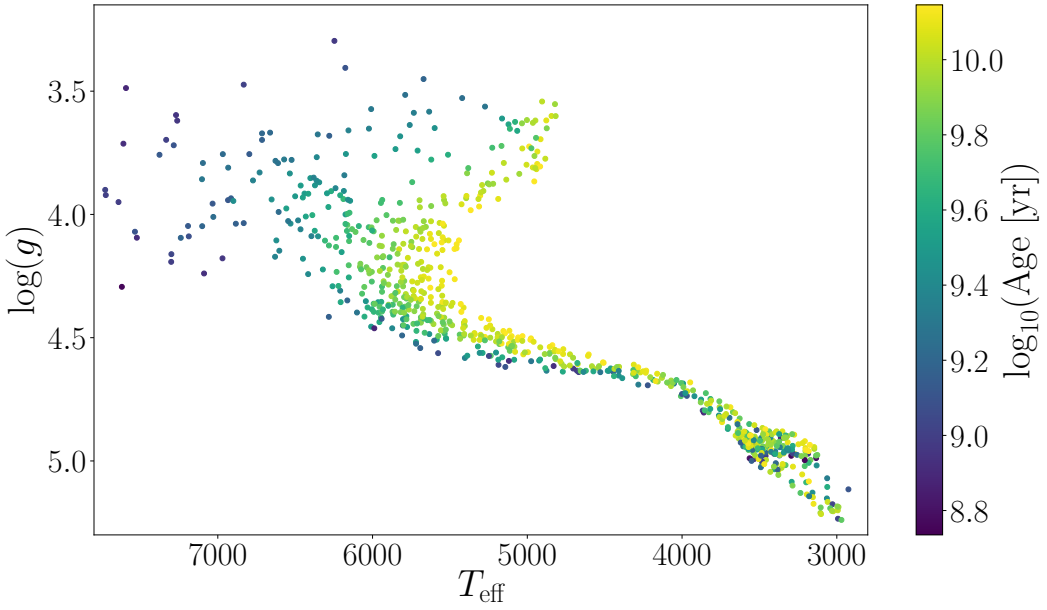

Fig. 4.— The true vs. predicted ages of stars. Ages calculated by combining gyrochronology and isochrone fitting are shown in color and ages calculated with isochrone fitting only are shown in gray. The five panels show the results for five different groups of stars: low *Ro* late F, GK and early M dwarfs, high *Ro* late F, GK and early M dwarfs, early F stars (B-V $<$ 0.45), late M dwarfs (B-V ¿ 1.4) and subgiants (EEP ¿ 454. Gyrochronology is highly effective for low *Ro* late F, GK and early M dwarfs and somewhat effective for high *Ro* late F, GK and early M dwarfs. It does not significantly improve ages for other groups of stars. Outliers are caused by multimodal posterior PDFs and imperfect MCMC sampling.

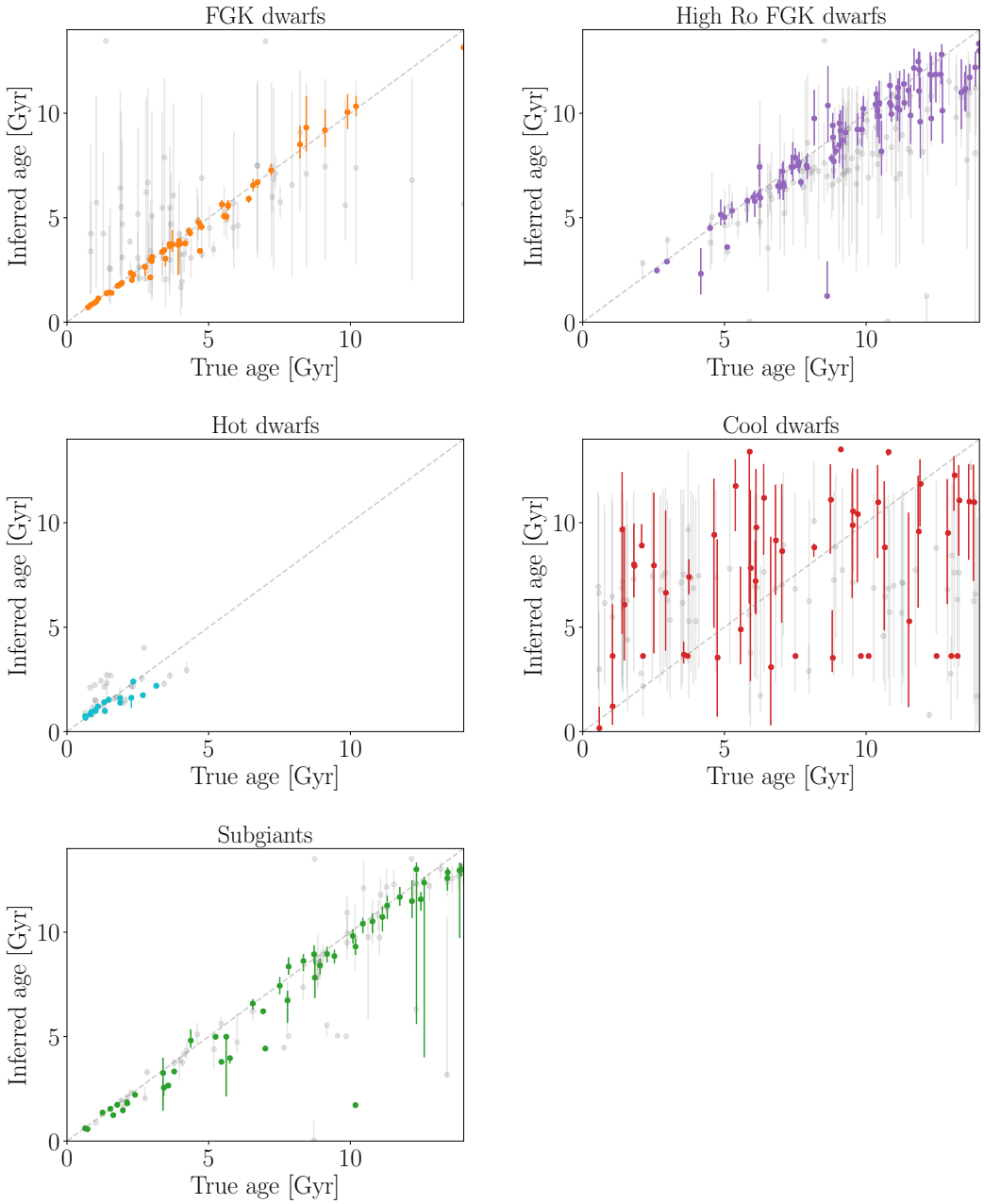

Fig. 5.— Simulated stars on an HR diagram, colored by the standard deviation of their age posterior PDFs, as a percentage of their ages. Gyrochronology is responsible for the high precision of ages measured for young FGK stars (stars in the upper left panel of figure 4. The ages of old FGK stars with Ro >2 are slightly less precise as these stars have stopped spinning down and their rotation periods are not information-rich. The ages of late M dwarfs are highly imprecise as these stars have not started spinning down.

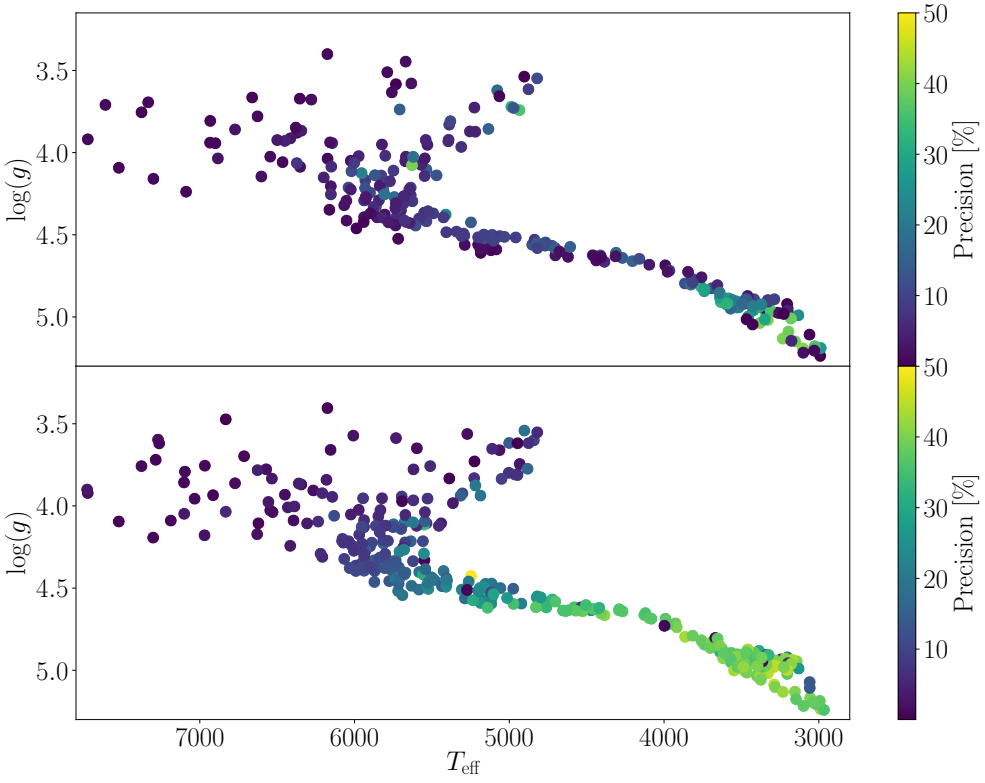

Fig. 6.— Posterior PDFs over the ages of members of the 650 Myr Praesepe cluster. The blue posteriors were recovered with `stardate`, by combining *Gaia* apparent magnitudes (G, G_BP and G_RP) and parallaxes with their photometric, *K2* rotation periods. The orange posteriors were obtained for the same stars using isochrone fitting with *Gaia*magnitudes and parallaxes. Each star was treated as a single field star. The blue posteriors are more tightly peaked and clustered around the true age of the cluster because rotation periods add age information. Combining gyrochronology and isochrone fitting provides more precise ages than isochrone fitting by itself.

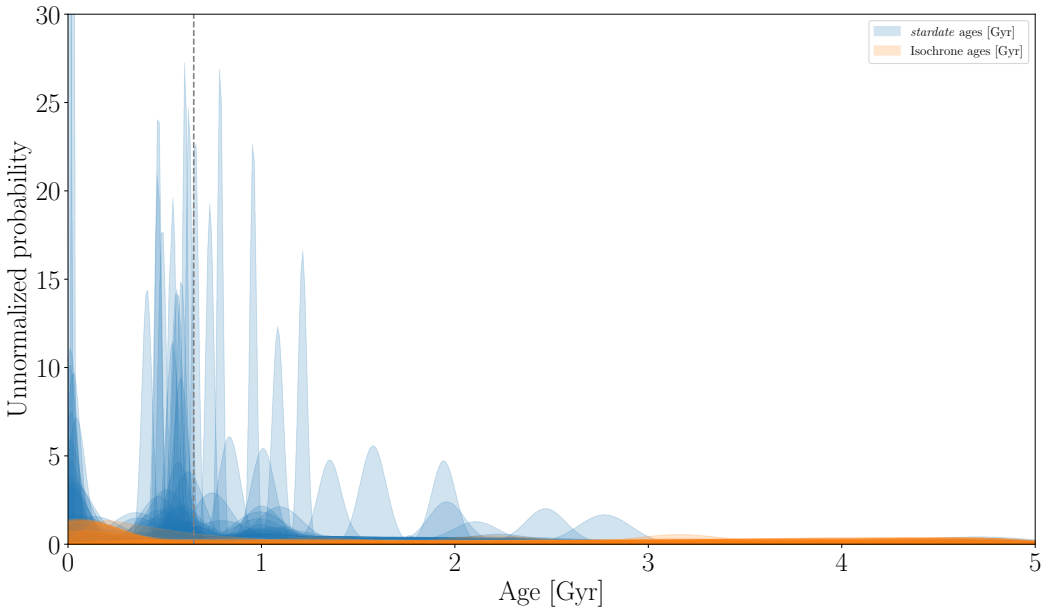

4. Discussion

In the previous sections we demonstrated that modeling the ages of stars using isochrones *and* gyrochronology can result in more precise and accurate ages than using isochrone fitting alone. Isochrone fitting and gyrochronology are complementary because gyrochronology is more precise where isochrone fitting is less precise (on the MS) and vice versa (at MS turn off). The method we present here is available as a *python* package called `stardate` which allows users to infer ages from their available apparent magnitudes, parallaxes, rotation periods and spectroscopic propertes in just a few lines of code. This method is applicable to an extremely large number of stars: late F, GK and early M stars with a rotation period and broad-band photometry. This already includes tens-of-thousands of *Kepler* and *K2* stars and could include millions more from *TESS*, *LSST*, *WFIRST*, *PLATO*, *Gaia*, and others in future. Although this method is designed for combining isochrone fitting with gyrochronology, `stardate` can still be used *without* rotation periods, in which case it will predict an isochrone-only stellar age. than the age of the Universe, and metallicities from -4 to 0.5. However, it is *optimally applicable* to stars with rotation periods, otherwise the result will be identical to ages measured with `isochrones.py`. However, `stardate` will often predict inaccurate ages for stars younger than around 500 million years, where stars are more likely to be rapidly rotating outliers, and close binaries whose interactions influence their rotation period evolution. Rotational outliers are often seen in clusters (see *e.g.* Douglas et al. 2016; Rebull et al. 2016; Douglas et al. 2017; Rebull et al. 2017) and many of these fall above the main sequence, indicating that they are binaries. When a star's age is not accurately represented by its rotation period, its isochronal age will be in tension with its gyrochronal one, however, given the high information content of gyrochronology, the gyrochronal age will dominate on the MS. In addition, measured rotation periods may not always be accurate and can, in many cases, be a harmonic of the true rotation period. A common rotation period measurement failure mode is to measure half the true rotation period. The best way to prevent an erroneous or outlying rotation period from resulting in an erroneous age measurement is to *allow* for outlying rotation periods using a mixture model. We intend to build a mixture model into `stardate` in future. As shown in figure 6, the gyrochronology model used here (Angus et al. 2015) does not provide a good fit to all available data. In future we intend to calibrate a new gyrochronology model that fits all available cluster and asteroseismic data. For now however, we simply warn users of these caveats and suggest that ages calculated using `stardate` are treated with appropriate caution.

5. Conclusion

We present a statistical framework for measuring precise ages of MS stars and subgiants by combining observables that relate, via different evolutionary processes, to stellar age. Specifically, we combined HR diagram/CMD placement with rotation periods, in a hierarchical Bayesian model, to age-date stars based on both their hydrogen burning and magnetic braking history. The two methods of isochrone fitting and gyrochronology were combined by taking the product of two likelihoods: one that contains an isochronal model and the other a gyrochronal one. We used the MIST stellar evolution models and computed isochronal ages and likelihoods using the `isochrones.py` *Python* package. The gyrochronal model was a power-law relation between rotation period, B-V color and age, based on the functional form first introduced by Barnes (2003) and later recalibrated by Angus et al. (2015), with a modification recommended by van Saders et al. (2016) that accounts for weakened magnetic braking at Rossby numbers larger than 2. We tested this age-dating method, implemented in a *Python* package called `stardate`, on simulated data and cluster stars. We demonstrated that combining gyrochronology with isochrone fitting produces age predictions that are an order of magnitude more precise than isochrone fitting alone. Gyrochronology and isochrone fitting are complementary: gyrochronology supplies precise ages on the main sequence and isochrone fitting provides precise ages near main sequence turn off. `stardate` allows users to infer precise ages for MS stars and subgiants alike, without having to first identify the age-dating method that is best for any given star. In addition, due to the flexibility of the `isochrones` package that `stardate` is built on top of, `stardate` accepts apparent magnitudes in all pass-bands covered by the MIST isochrones which includes the Johnson-Cousins, *2MASS*, *Kepler*, *SDSS* and *Gaia* photometric systems. However, we caution users that the gyrochronology model currently built into `stardate` does not alway provide a good fit to all data and is not suitable for very young stars or binaries. In the future we hope to make several improvements to the gyrochronology relation implemented in `stardate` that will make it applicable to *all* MS and subgiant stars.

The code used in this project is available as a documented *python* package called `stardate`. It is available for download via Github[13] or through PyPI[14]. Documentation is available at https://stardate.readthedocs.io/en/latest/. All code used to produce the figures in this paper is available at https://github.com/RuthAngus/stardate. add github hash and Zenodo doi.

[13] git clone https://github.com/RuthAngus/stardate.git

[14] pip install stardate_code

Some of the data presented in this paper were obtained from the Mikulski Archive for Space Telescopes (MAST). STScI is operated by the Association of Universities for Research in Astronomy, Inc., under NASA contract NAS5-26555. Support for MAST for non-HST data is provided by the NASA Office of Space Science via grant NNX09AF08G and by other grants and contracts. This paper includes data collected by the Kepler mission. Funding for the *Kepler* mission is provided by the NASA Science Mission directorate.

This work made use of the gaia-kepler.fun crossmatch database created by Megan Bedell

This work has made use of data from the European Space Agency (ESA) mission *Gaia* (`https://www.cosmos.esa.int/gaia`), processed by the *Gaia* Data Processing and Analysis Consortium (DPAC, `https://www.cosmos.esa.int/web/gaia/dpac/consortium`). Funding for the DPAC has been provided by national institutions, in particular the institutions participating in the *Gaia* Multilateral Agreement.

6. Appendix

Priors

We used the default priors in the `isochrones.py` *python* package. The prior over age was,

$$p(A) = \frac{\log(10)10^A}{10^{10.5} - 10^8}, \quad 8 < A < 10.5. \tag{17}$$

where A, is $\log_{10}$(Age [yrs]). The prior over EEP was uniform with an upper limit of 800. We found that adding this upper limit reduced some multi-modality caused by the giant branch and resulted in better performance. The prior over true bulk metallicity was based on the galactic metallicity distribution, as inferred using data from the Sloan Digital Sky Survey citation. It is the product of a Gaussian that describes the metallicity distribution over halo stars and two Gaussians that describe the metallicity distribution in the thin and thick disks:

$$\begin{aligned} p(F) = & \quad H_F \frac{1}{\sqrt{2\pi\sigma^2_{\rm halo}}} \exp\left(-\frac{(F-\mu_{\rm halo})^2}{2\sigma_{\rm halo}}\right) \\ & \times(1-H_F)\frac{1}{\xi}\left[\frac{0.8}{0.15}\exp\left(-\frac{(F-0.016)^2}{2\times0.15^2}\right) + \frac{0.2}{0.22}\exp\left(-\frac{(F-0.15)^2}{2\times0.22^2}\right)\right], \end{aligned} \tag{18}$$

where $H_F = 0.001$ is the halo fraction, $\mu_{\rm halo}$ and $\sigma_{\rm halo}$ are the mean and standard deviation of a Gaussian that describes a probability distribution over metallicity in the halo, and take values -1.5 and 0.4 respectively. The two Gaussians inside the square brackets describe probability distributions over metallicity in the thin and thick disks. The values of the means and standard deviations in these Gaussians are from **?**. ξ is the integral of everything in the square brackets from $-\infty$ to ∞ and takes the value ~ 2.507. The prior over distance was,

$$p(D) = \frac{3}{3000^3}D^2, \quad 0 < D < 3000, \tag{19}$$

with D in kiloparsecs, and, finally, the prior over extinction was uniform between zero and one,

$$p(A_V) = U(0, 1). \tag{20}$$

REFERENCES

R. Angus, S. Aigrain, D. Foreman-Mackey, and A. McQuillan. Calibrating gyrochronology using Kepler asteroseismic targets. *MNRAS*, 450:1787–1798, June 2015. doi: 10.1093/mnras/stv423.

S. A. Barnes. On the Rotational Evolution of Solar- and Late-Type Stars, Its Magnetic Origins, and the Possibility of Stellar Gyrochronology. *ApJ*, 586:464–479, March 2003. doi: 10.1086/367639.

S. A. Barnes. Ages for Illustrative Field Stars Using Gyrochronology: Viability, Limitations, and Errors. *ApJ*, 669:1167–1189, November 2007. doi: 10.1086/519295.

C. J. Burke, J. L. Christiansen, F. Mullally, S. Seader, D. Huber, J. F. Rowe, J. L. Coughlin, S. E. Thompson, J. Catanzarite, B. D. Clarke, T. D. Morton, D. A. Caldwell, S. T. Bryson, M. R. Haas, N. M. Batalha, J. M. Jenkins, P. Tenenbaum, J. D. Twicken, J. Li, E. Quintana, T. Barclay, C. E. Henze, W. J. Borucki, S. B. Howell, and M. Still. Terrestrial Planet Occurrence Rates for the Kepler GK Dwarf Sample. *ApJ*, 809:8, August 2015. doi: 10.1088/0004-637X/809/1/8.

J. Choi, A. Dotter, C. Conroy, M. Cantiello, B. Paxton, and B. D. Johnson. Mesa Isochrones and Stellar Tracks (MIST). I. Solar-scaled Models. *ApJ*, 823:102, June 2016. doi: 10.3847/0004-637X/823/2/102.

A. Dotter. MESA Isochrones and Stellar Tracks (MIST) 0: Methods for the Construction of Stellar Isochrones. *ApJS*, 222:8, January 2016. doi: 10.3847/0067-0049/222/1/8.

A. Dotter, B. Chaboyer, D. Jevremović, V. Kostov, E. Baron, and J. W. Ferguson. The Dartmouth Stellar Evolution Database. *ApJS*, 178:89–101, September 2008. doi: 10.1086/589654.

S. T. Douglas, M. A. Agüeros, K. R. Covey, P. A. Cargile, T. Barclay, A. Cody, S. B. Howell, and T. Kopytova. K2 Rotation Periods for Low-mass Hyads and the Implications for Gyrochronology. *ApJ*, 822:47, May 2016. doi: 10.3847/0004-637X/822/1/47.

S. T. Douglas, M. A. Agüeros, K. R. Covey, and A. Kraus. Poking the Beehive from Space: K2 Rotation Periods for Praesepe. *ApJ*, 842:83, June 2017. doi: 10.3847/1538-4357/aa6e52.

D. W. Evans, M. Riello, F. De Angeli, G. Busso, F. van Leeuwen, C. Jordi, C. Fabricius, A. G. A. Brown, J. M. Carrasco, H. Voss, M. Weiler, P. Montegriffo, C. Cacciari, P. Burgess, and P. Osborne. Gaia Data Release 1. Validation of the photometry. *A&A*, 600:A51, April 2017. doi: 10.1051/0004-6361/201629241.

D. Foreman-Mackey, D. W. Hogg, D. Lang, and J. Goodman. emcee: The MCMC Hammer. *PASP*, 125:306, March 2013. doi: 10.1086/670067.

D. Foreman-Mackey, D. W. Hogg, and T. D. Morton. Exoplanet Population Inference and the Abundance of Earth Analogs from Noisy, Incomplete Catalogs. *ApJ*, 795:64, November 2014. doi: 10.1088/0004-637X/795/1/64.

L. Fossati, S. Bagnulo, J. Landstreet, G. Wade, O. Kochukhov, R. Monier, W. Weiss, and M. Gebran. The effect of rotation on the abundances of the chemical elements of the A-type stars in the Praesepe cluster. *A&A*, 483:891–902, June 2008. doi: 10.1051/0004-6361:200809467.

Gaia Collaboration, A. G. A. Brown, A. Vallenari, T. Prusti, J. H. J. de Bruijne, C. Babusiaux, C. A. L. Bailer-Jones, M. Biermann, D. W. Evans, L. Eyer, and et al. Gaia Data Release 2. Summary of the contents and survey properties. *A&A*, 616:A1, August 2018. doi: 10.1051/0004-6361/201833051.

Daniel Huber, Stephen T. Bryson, Michael R. Haas, Thomas Barclay, Geert Barentsen, Steve B. Howell, Sanjib Sharma, Dennis Stello, and Susan E. Thompson. The K2 Ecliptic Plane Input Catalog (EPIC) and Stellar Classifications of 138,600 Targets in Campaigns 1-8. *The Astrophysical Journal Supplement Series*, 224:2, May 2016. doi: 10.3847/0067-0049/224/1/2.

J. Irwin and J. Bouvier. The rotational evolution of low-mass stars. In E. E. Mamajek, D. R. Soderblom, and R. F. G. Wyse, editors, *The Ages of Stars*, volume 258 of *IAU Symposium*, pages 363–374, June 2009. doi: 10.1017/S1743921309032025.

S. D. Kawaler. Angular momentum loss in low-mass stars. *ApJ*, 333:236–247, October 1988. doi: 10.1086/166740.

S. D. Kawaler. Rotational dating of middle-aged stars. *ApJ*, 343:L65–L68, August 1989. doi: 10.1086/185512.

E. E. Mamajek and L. A. Hillenbrand. Improved Age Estimation for Solar-Type Dwarfs Using Activity-Rotation Diagnostics. *ApJ*, 687:1264–1293, November 2008. doi: 10.1086/591785.

A. W. Mann, E. Gaidos, A. Vanderburg, A. C. Rizzuto, M. Ansdell, J. V. Medina, G. N. Mace, A. L. Kraus, and K. R. Sokal. Zodiacal Exoplanets in Time (ZEIT). IV. Seven Transiting Planets in the Praesepe Cluster. *AJ*, 153:64, February 2017. doi: 10.1088/1361-6528/aa5276.

A. W. Mann, A. Vanderburg, A. C. Rizzuto, A. L. Kraus, P. Berlind, A. Bieryla, M. L. Calkins, G. A. Esquerdo, D. W. Latham, G. N. Mace, N. R. Morris, S. N. Quinn, K. R. Sokal, and R. P. Stefanik. Zodiacal Exoplanets in Time (ZEIT). VI. A Three-planet System in the Hyades Cluster Including an Earth-sized Planet. *AJ*, 155:4, January 2018. doi: 10.3847/1538-3881/aa9791.

S. P. Matt, K. B. MacGregor, M. H. Pinsonneault, and T. P. Greene. Magnetic Braking Formulation for Sun-like Stars: Dependence on Dipole Field Strength and Rotation Rate. *ApJ*, 754:L26, August 2012. doi: 10.1088/2041-8205/754/2/L26.

S. P. Matt, A. S. Brun, I. Baraffe, J. Bouvier, and G. Chabrier. The Mass-dependence of Angular Momentum Evolution in Sun-like Stars. *ApJ*, 799:L23, January 2015. doi: 10.1088/2041-8205/799/2/L23.

A. McQuillan, T. Mazeh, and S. Aigrain. Rotation Periods of 34,030 Kepler Main-sequence Stars: The Full Autocorrelation Sample. *ApJS*, 211:24, April 2014. doi: 10.1088/0067-0049/211/2/24.

B. Paxton, L. Bildsten, A. Dotter, F. Herwig, P. Lesaffre, and F. Timmes. Modules for Experiments in Stellar Astrophysics (MESA). *ApJS*, 192:3, January 2011. doi: 10.1088/0067-0049/192/1/3.

B. Paxton, M. Cantiello, P. Arras, L. Bildsten, E. F. Brown, A. Dotter, C. Mankovich, M. H. Montgomery, D. Stello, F. X. Timmes, and R. Townsend. Modules for Experiments in Stellar Astrophysics (MESA): Planets, Oscillations, Rotation, and Massive Stars. *ApJS*, 208:4, September 2013. doi: 10.1088/0067-0049/208/1/4.

B. Paxton, P. Marchant, J. Schwab, E. B. Bauer, L. Bildsten, M. Cantiello, L. Dessart, R. Farmer, H. Hu, N. Langer, R. H. D. Townsend, D. M. Townsley, and F. X. Timmes. Modules for Experiments in Stellar Astrophysics (MESA): Binaries, Pulsations, and Explosions. *ApJS*, 220:15, September 2015. doi: 10.1088/0067-0049/220/1/15.

B. Paxton, J. Schwab, E. B. Bauer, L. Bildsten, S. Blinnikov, P. Duffell, R. Farmer, J. A. Goldberg, P. Marchant, E. Sorokina, A. Thoul, R. H. D. Townsend, and F. X. Timmes. Modules for Experiments in Stellar Astrophysics (MESA): Convective Boundaries, Element Diffusion, and Massive Star Explosions. *ApJS*, 234:34, February 2018. doi: 10.3847/1538-4365/aaa5a8.

E. A. Petigura, A. W. Howard, and G. W. Marcy. Prevalence of Earth-size planets orbiting Sun-like stars. *Proceedings of the National Academy of Science*, 110:19273–19278, November 2013. doi: 10.1073/pnas.1319909110.

L. M. Rebull, J. R. Stauffer, J. Bouvier, A. M. Cody, L. A. Hillenbrand, D. R. Soderblom, J. Valenti, D. Barrado, H. Bouy, D. Ciardi, M. Pinsonneault, K. Stassun, G. Micela, S. Aigrain, F. Vrba, G. Somers, J. Christiansen, E. Gillen, and A. Collier Cameron. Rotation in the Pleiades with K2. I. Data and First Results. *AJ*, 152:113, November 2016. doi: 10.3847/0004-6256/152/5/113.

L. M. Rebull, J. R. Stauffer, L. A. Hillenbrand, A. M. Cody, J. Bouvier, D. R. Soderblom, M. Pinsonneault, and L. Hebb. Rotation of Late-type Stars in Praesepe with K2. *ApJ*, 839:92, April 2017. doi: 10.3847/1538-4357/aa6aa4.

A. C. Rizzuto, A. Vanderburg, A. W. Mann, A. L. Kraus, C. D. Dressing, M. A. Agüeros, S. T. Douglas, and D. M. Krolikowski. Zodiacal Exoplanets in Time (ZEIT). VIII. A Two-planet System in Praesepe from K2 Campaign 16. *AJ*, 156:195, November 2018. doi: 10.3847/1538-3881/aadf37.

A. Skumanich. Time Scales for CA II Emission Decay, Rotational Braking, and Lithium Depletion. *ApJ*, 171:565, February 1972. doi: 10.1086/151310.

D. R. Soderblom. The Ages of Stars. *ARA&A*, 48:581–629, September 2010. doi: 10.1146/annurev-astro-081309-130806.

J. L. van Saders and M. H. Pinsonneault. Fast Star, Slow Star; Old Star, Young Star: Subgiant Rotation as a Population and Stellar Physics Diagnostic. *ApJ*, 776:67, October 2013. doi: 10.1088/0004-637X/776/2/67.

J. L. van Saders, T. Ceillier, T. S. Metcalfe, V. Silva Aguirre, M. H. Pinsonneault, R. A. García, S. Mathur, and G. R. Davies. Weakened magnetic braking as the origin of anomalously rapid rotation in old field stars. *Nature*, 529:181–184, January 2016. doi: 10.1038/nature16168.

A. Vanderburg, A. W. Mann, A. Rizzuto, A. Bieryla, A. L. Kraus, P. Berlind, M. L. Calkins, J. L. Curtis, S. T. Douglas, G. A. Esquerdo, M. E. Everett, E. P. Horch, S. B. Howell, D. W. Latham, A. W. Mayo, S. N. Quinn, N. J. Scott, and R. P. Stefanik. Zodiacal Exoplanets in Time (ZEIT). VII. A Temperate Candidate Super-Earth in the Hyades Cluster. *AJ*, 156:46, August 2018. doi: 10.3847/1538-3881/aac894.

D. Veras, D. J. A. Brown, A. J. Mustill, and D. Pollacco. Prospects for detecting decreasing exoplanet frequency with main-sequence age using PLATO. *MNRAS*, 453:67–72, October 2015. doi: 10.1093/mnras/stv1615.

N. J. Wright, J. J. Drake, E. E. Mamajek, and G. W. Henry. The Stellar-activity-Rotation Relationship and the Evolution of Stellar Dynamos. *ApJ*, 743:48, December 2011. doi: 10.1088/0004-637X/743/1/48.

S. Yi, P. Demarque, Y.-C. Kim, Y.-W. Lee, C. H. Ree, T. Lejeune, and S. Barnes. Toward Better Age Estimates for Stellar Populations: The Y^2 Isochrones for Solar Mixture. *ApJS*, 136:417–437, October 2001. doi: 10.1086/321795.